Journal of Engineering Science 15(1), 2024, 75-81
DOI: https://doi.org/10.3329/jes.v15i1.76044

JES
an international Journal

EFFECT OF CALCINATION TEMPERATURE ON THE SURFACE OF PREPARED ZnO NANOCATALYSTS

Mohammad Akter Hossain[1,2], Md. Nazmul Kayes[3*], Md. Mufazzal Hossain[1]

[1]Department of Chemistry, University of Dhaka, Dhaka 1000, Bangladesh
[2]Department of Chemistry and Biochemistry, Kent State University, OH 44240, USA
[3]Department of Chemistry, University of Barishal, Barishal 8254, Bangladesh

Received: 09 April 2024 Accepted: 30 May 2024

ABSTRACT

ZnO nanoparticles (NPs) having nsemiconducting properties are important nanocatalysts for many surface reactions. Because of their extensive use as heterogeneous nanocatalyst for energy production and environmental cleaning, it is essential to understand their surface properties to design better chemical and photochemical nanocatalysts. Here, we used the sol-gel method to develop numerous ZnO NPs at various calcination temperatures (300 - 800 °C) and analyzed by different surface characterization techniques such as FTIR, SEM, XRD and UV-visible absorption spectroscopy. To investigate the catalytic activity a series of photooxidation studies on Remazol Red RR (RRR) were carried out at different conditions. From the surface characteristic analysis, it is found that the crystalline ZnO NPs are formed at above 400 °C temperature. The highest photocatalytic efficiency is found at 500 °C which might be related to the lowest particle size (35.4 ± 5.2 nm) and surface heterogeneity. The experimental results suggest that temperature-controlled growth rate and intra/inter-particle heterogeneity of ZnO nanoparticles have a great impact on the surface properties and photocatalytic activity. In addition to surface area, surface defects and crystal deformation may have a considerable impact on the photocatalytic activity by ZnO NPs. Finally, this study will help to understand what type of surface properties need to optimize to design industrial suit ZnO nanocatalysts.

Keywords*: Calcination temperature, heterogeneous catalysis, nanocatalyst, Remazol red RR and ZnO.*

1. INTRODUCTION

Nowadays, heterogeneous nanocatalysts are cutting-edge materials with significant economic and social implications. Because of their facile surface tuning capability, they have a wide range of applications in energy production, environmental cleansing, antimicrobial activity, and probing single-molecule catalysis (Xu W. *et al.*, 2008; Khan S. T. *et al.*, 2015; Ani I. J. *et al.*, 2018; Velusamy K. *et al.*, 2021, Ghosh N. *et al.*, 2024). Heterogeneous metal nanocatalysts like Cu, Ni and Pd NPs are used in a variety of hydrogenation processes in the chemical industry while noble metal nanocatalysts such as Au NPs are widely used in different oxidation processes (Bond G. C. *et al.*, 1999; Wang L.-X. *et al.*, 2020; Lévay K. *et al.*, 2020). The extraordinary catalytic activity of this noble metal is enhanced by the quantum confinement effect. Moreover, because of the photostability, low cost, and nontoxicity semiconducting metal oxide nanocatalysts such as ZnO and TiO_2 act as a better photocatalyst for clean energy production and pollution control (Qin H. *et al.*, 2011; Hossain M. M. *et al.*, 2014; Ng K. H. *et al.*, 2019; Bakbolat B. *et al.*, 2020, Khalid A. *et al.*, 2023, Etafo N. O. *et al.*, 2024). Their persistent surface-active sites and right facet of substrate interaction provide an efficient catalysis performance. However, the surface structure of nanoparticles, which is controlled by the calcination temperature, has a substantial impact on this activity (Mountrichas G. *et al.*, 2014; Venu Gopal V. R. *et al.*, 2017; Dassanayake A. C. *et al.*, 2019; Lal M. *et al.*, 2021).

For effective applications of ZnO NPs, people employ a variety of processes for their synthesis, including the metallurgical process, mechanochemical process, controlled precipitation, sol-gel method, and the hydrothermal approach followed by calcination at various high temperatures (Kołodziejczak-Radzimska A. and Jesionowski T., 2014). This temperature plays a key factor in controlling the growth rate of ZnO nanocrystals, which regulates their surface properties mainly surface area, surface defects and band gap energy (Kumar S. *et al.*, 2012; Kayani Z. N. *et al.*, 2015; Clarke B. *et al.*, 2023). However, other surface properties such as surface facets, intra and inter-particle heterogeneity, and tensile strain can also be regulated by growth rate and influence the catalysis activity.

*Corresponding Author: *dmnkayes@bu.ac.bd*

ISSN 2075-4914 (print); ISSN 2706-6835 (online)

In this study, we prepared ZnO NPs through the sol-gel method at various calcination temperatures and characterized by UV-visible absorption spectroscopy, FTIR, SEM and XRD. According to characterization, we found that their surface morphology significantly changes with temperature. Here we tried to describe in detail what type of distinct surface features can be changed with temperature and what is their contribution in heterogeneous photochemical catalysis. To assess the photocatalytic efficiency of ZnO NPs synthesized at different calcination temperatures, we carried out a series of photodegradation experiments using RRR, an industrial carcinogenic dye.

2. EXPERIMENTAL

The preparation method is described elsewhere (Hossain M. A. *et al.*, 2021). Shortly, zinc acetate dihydrate (~ 11 g) and oxalic acid dihydrate (12.5 g) were dissolved in 200 - 300 mL ethanol at 60 and 50 ^{o}C, respectively. A thick gel was formed after mixing them slowly, dried at 80 °C for 20 hours and then calcined for 2 hours at 300, 400, 500, 600, and 800^{o}C, respectively. To investigate the surface heterogeneity, the prepared ZnO nanoparticles were then characterized by UV-visible and IR spectroscopy, SEM, EDX and XRD.

The prepared ZnO NPs were first identified using a Shimadzu UV-1800 UV-Vis Spectrophotometer. The absorption spectra of ZnO NPs were recorded in an aqueous suspension after 15 minutes of pre-sonication. They were then characterized by a Shimadzu FTIR-8300 spectrophotometer for surface impurity analysis. A pallet was made by mixing a tiny amount of ZnO NPs with KBr powder, which was then directly used to get FTIR absorption spectrum. To evaluate the surface morphology and particle size several images of ZnO NPs were taken by SEM (Model: JSM-6490, JEOL) under high vacuum condition. ImageJ tool was used to evaluate the particle size from SEM images. With monochromatic Cu kα1 radiation (λ=1.540598 Å), the powder X-ray pattern was captured with a Philips PW 1724 X-ray 700 generator and an XDC-700 GuinierHägg focusing camera. The diffraction pattern was recorded in an image plate after a 15-minute exposure at 40kv-30 mA. An HD-CR 35 NDT scanner was used to scan the image plates. The intensity of diffracted X-rays as a function of 2θ is detected by a diffraction plot. Finally, they were used to produce a nano ZnO film to be used as a photocatalyst.

Nano ZnO film was developed from the drop casting of an aqueous suspension of ZnO NPs on a microscopic slide (Kayes M. N. *et al.*, 2016). It was then used for the photooxidation of RRR (Hariharan C. *et al.*, 2006). During an experiment, it was dipped in an aqueous solution of RRR in a reactor. Waited for adsorption equilibrium time and then applied light irradiation under continuous stirring. The absorption data were recorded over photocatalysis time utilizing a Shimadzu UV-1800 UV-Vis Spectrophotometer.

3. RESULTS AND DISCUSSIONS

3.1 Characterization by UV-Visible Spectroscopy

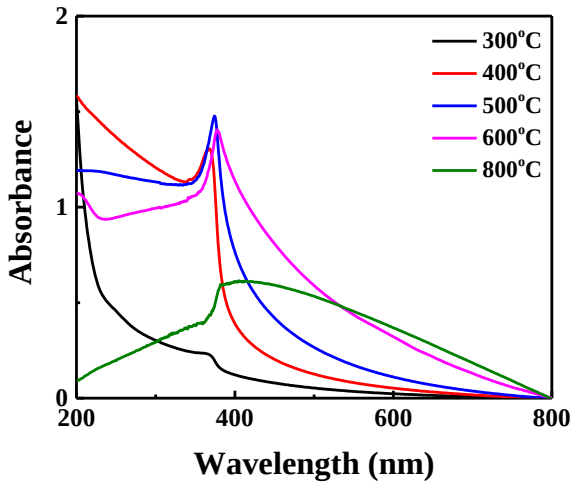

Figure 1. UV-Visible absorption spectra of ZnO NPs synthesized at different calcination temperatures

The UV-visible absorption spectrum reveals the quantum confinement efficiency of nanoparticles, including particle size, band gap and inter-particle heterogeneity from the sharpness of their peaks. Figure 1 shows the UV-visible absorbance of different growth ZnO NPs. Due to excitonic absorption from oxide nanoparticles, a sharp peak is generated at λ_{max} 368, 374 and 377 nm with a band gap energy of 3.33 ± 0.03 eV for calcination temperature of 400, 500 and 600^{o}C, respectively. Furthermore, at 800 ^{o}C, a broad peak at λ_{max} 395 nm is shown for growing

ZnO NPs, whereas at 300 ºC, it is insignificant. This hypsochromic shift of λ_{max} indicates the presence of quantum confinement properties in the nanoparticles. As the particle size decreases, absorption peak shifts to the lower wavelength region, resulting in increased quantum confinement with high band gap energy (Lin K.-F. *et al.*, 2005; Lin K.-F. *et al.*, 2006). These changes in particle size as a function of temperature provide basic assumptions of inter-particle heterogeneity, which can play a significant impact on the catalytic activity of nanoparticles (Figure 5).

3.2 Characterization by FTIR Analysis

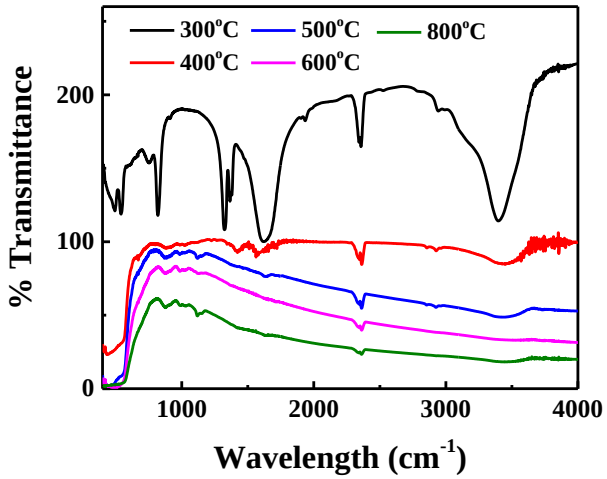

Figure 2. FTIR absorption spectra of ZnO NPs synthesized at different calcination temperatures

The FTIR absorption spectra of different ZnO NPs as pressed KBr pellets were captured using a Shimadzu FTIR-8300 spectrophotometer at room temperature. Figure 2 shows the spectra results of them at various calcination temperatures. The materials contain carboxylate and hydroxyl impurities, as evidenced by a sequence of absorption peaks ranging from 400 to 4000 cm^{-1}. The O–H stretching mode of the hydroxyl group, which is also accessible in commercial ZnO powder, was assigned a broad band at 3432 cm^{-1} (Hossain M. A. *et al.*, 2021). The peaks at 1630 to 819 cm^{-1} are caused by asymmetrical and symmetrical stretching of the zinc carboxylate (Xiong G. *et al.*, 2006). Interestingly, the spectral fingerprints of carboxylate impurities disappear as the calcination temperature increases, implying that zinc carboxylate dissociates to ZnO. With increasing calcination temperature, a distinctive band appears at 440 cm^{-1} that corresponds to the E2 mode of hexagonal ZnO (Kaschner A. *et al.*, 2002). Finally, it can be concluded that ZnO prepared at temperatures above 400 ºC maintains purity with a lower surface coverage of the hydroxyl group.

3.3 Characterization by SEM Image

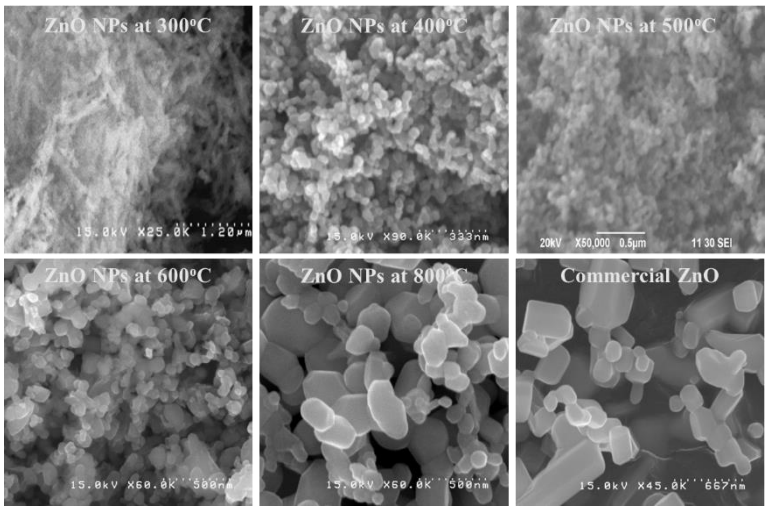

Figure 3. SEM images of ZnO NPs synthesized at different calcination temperatures

SEM image better displays the particle heterogeneity by providing the information of morphology and crystallinity. Figure 3 displays SEM images of commercial ZnO and growth ZnO NPs at different calcination temperatures. We also applied the ImageJ tools to estimate the average particle size from the SEM image which is demonstrated in Table 1 (Collins T. J., 2007). Temperature plays a significant impact on the size and shape of nanoparticles. As temperature increases, the size of the nanoparticles increases due to their agglomeration. Moreover, there is a phase transition from amorphous to crystalline with increasing temperature. Below 400 ^{o}C majority of the particles are in amorphous phase whereas it undergoes crystallinity above this temperature. At 400 - 500 ^{o}C, nanoparticles are essentially identical in size and shape, however at 800 ^{o}C, they resemble commercial hexagonal ZnO shapes with larger size. Different crystalline shapes and size of the nanoparticles indicate temperature-controlled growth rate dictating the intra and inter-particle heterogeneity of the nanoparticles. The inter-particle heterogeneity can be confirmed from the size difference derived from different calcination temperatures, as well as the broad distribution (standard deviation) of particle size for each calcination temperature (Table 1). This intrinsic heterogeneity can influence the catalytic activity of nanoparticles (Zhou X. *et al.*, 2010). Furthermore, EDX was used to examine the chemical composition of the growth ZnO NPs. It asserts that except for Zn and O atoms there are no impurities in the surface above 400 ^{o}C calcination.

Table 1. Estimation of the size of ZnO nanoparticles prepared at various calcination temperatures

Catalyst	Calcination temperature (^{o}C)	Particle size distribution / nm
ZnO NPs	300	amorphous
ZnO NPs	400	40.8 ± 8.6
ZnO NPs	500	35.4 ± 5.2
ZnO NPs	600	69.3 ± 8.2
ZnO NPs	800	85.9 ± 7.8 (small) 190 ± 8 (large)
Commercial ZnO	-	130 ± 8 (small) ~ 500 nm (large)

3.4 Characterization by XRD Analysis

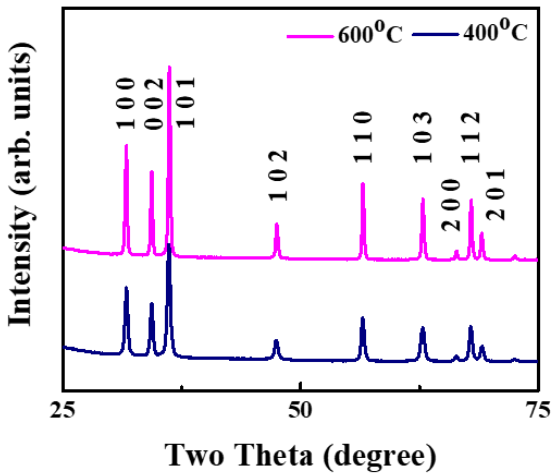

Figure 4. XRD pattern of ZnO NPs synthesized at different calcination temperatures

The crystallinity of ZnO NPs is also confirmed from XRD. A typical example of XRD the growth ZnO NPs calcined at 400 and 600 ^{o}C are shown in Figure 4. It was found that the Bragg's peaks indexed, and their intensities matched the JCPDS data of zincite (JCPDS 36-1451). It confirms that growing ZnO NPs have hexagonal wurtzite crystalline structures (Kaschner A. *et al.*, 2002; Chen C. *et al.*, 2011). Using the Debye-Scherrer formula, the crystalline size of growth ZnO NPs were determined from the X-ray line broadening of the XRD peak corresponding to (0 0 2) reflection (Aneesh N. P. M. *et al.*, 2007). Moreover, crystalline ZnO NPs have different surface planes with different surface stress and energy (Tang Z. *et al.*, 2020). The contribution of each plane should be distinct, suggesting that intra-particle heterogeneity in ZnO nanoparticles is feasible. Also, crystal deformation of ZnO can also be observed in SEM image due to lattice mismatch during growth of ZnO

nanocrystal, which introduces local strain effect and creates intrinsic surface heterogeneity (Bindu P. *et al.*, 2014; Tsai C.-Y. *et al.*, 2017).

3.5 Photocatalytic Activity

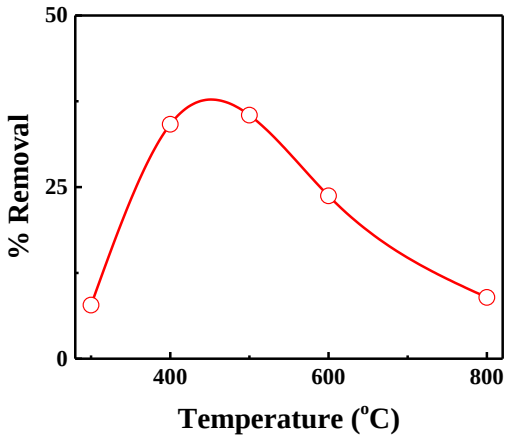

Figure 5. Temperature dependent heterogeneous catalysis of ZnO NPs for oxidative elimination of RRR. All reactions were carried out for 70 minutes in the presence of 0.1 mM RRR and an identical amount (0.115g) of ZnO NPs suspension under sunlight irradiation.

To demonstrate the effect of calcination temperature on the growth of ZnO NPs, we used heterogeneous photocatalysis on RRR oxidation. RRR is an industrial pollutant which undergoes photocatalytic degradation by ZnO NPs in presence of light irradiation. To mineralize the RRR by ZnO NPs we previously verified the effect of catalyst dose (0.115g), reaction time (70 minutes), initial RRR concentration (1.0×10^{-4} M) and light sources (sunlight) at calcination temperature of 500 °C (Hossain M. A. *et al.*, 2021). However, photocatalysis of ZnO NPs is not equal to all calcination temperatures. Figure 5 shows the activity comparison of heterogeneous photocatalysis of ZnO NPs. The maximum photocatalytic activity is obtained at 500 °C calcination temperature of ZnO NPs. This is due to their available high surface area, high surface energy and possible intrinsic surface defects. However, photocatalytic activity drops above and below optimal temperature because of decreasing surface area and deviation of crystalline properties of ZnO NPs, respectively. Scheme 1 depicts the mechanism of photocatalytic activity of ZnO NPs on RRR oxidation (Ong C. B. *et al.*, 2018; Hossain M. A. *et al.*, 2021).

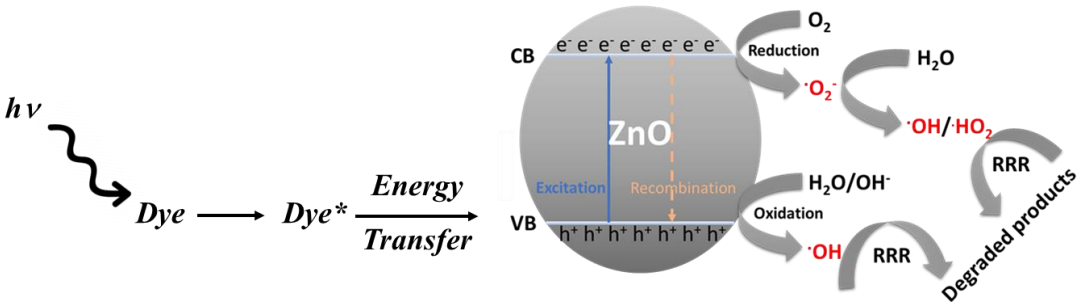

Scheme 1. The photocatalytic mechanism of ZnO nanoparticle under sunlight irradiation.

Because of high band gap energy (3.0-3.2 eV) ZnO NPs experienced high charge separation under UV light irradiation by producing energetic holes and excited electrons. Both were reacted with water and dissolved oxygen molecules in the environment. Energetic holes were reduced by H_2O molecules or hydroxide ions (OH^-) to produce hydroxyl radicals (•OH), whereas excited electrons were oxidized by dissolved O_2 to produce superoxide radicals ($\bullet O_2^-$), which further protonated to hydroperoxyl radical ($HO_2\bullet$)/ Hydrogen peroxide (H_2O_2) and later produced hydroxyl radicals. These radicals are highly active oxygen species that degrade the organic dyes in order to reduce pollution. Under sunlight irradiation, the dye is initially excited and then transfers energy to the photocatalyst (ZnO NPs). The other reactions are almost the same as UV light irradiation (Kayes M. N. *et al.*, 2016). Furthermore, we synthesized the ZnO NPs under harsh conditions which increase the probability of intrinsic surface defects. Because high temperatures accelerate the formation rate of nanoparticles, which incorporate more surface defects (Liu P. S. and Chen G. F., 2014). These surface defects assist to lower the band gap energy while

increasing catalytic rate (Roth A. P. *et al.*, 1982; Xu J. *et al.*, 2016). The number of surface defects grows until the temperature reaches its optimum (500^{o}C), after which it reduces due to either decreased surface area or surface destruction at high temperatures. However, the influence of individual crystal plane or lattice mismatch on catalysis cannot be investigated using this ensemble averaging method. It is entirely achievable using a single-molecule method, which will be the focus of our future research.

4. CONCLUSIONS

Other than surface area, the surface heterogeneity of ZnO NPs can also affect the photocatalysis which might be regulated by growth rate of ZnO NPs, surface defects, surface energy, local strain effect, *etc.* Our current approaches can explain some of them such as growth rate and averaged inter-particle heterogeneous catalysis of ZnO NPs, but not intra-particle heterogeneous catalysis, which requires a single-molecule method. Overall, based on the investigation of surface characterization and catalytic application we were able to identify various parameters other than surface area which are important information to design a better ZnO nanocatalyst.

ACKNOWLEDGEMENT

One of the authors (MMH) acknowledges the financial support from the Ministry of Education, Bangladesh.

REFERENCES

Aneesh N. P. M., Vanaja K. A., Jayaraj M. K., 2007. Synthesis of ZnO nanoparticles by hydrothermal method, In *Proc. SPIE*, 6639, Nanophotonic Materials IV, 66390J1-9 .

Ani I. J., Akpan U. G., Olutoye M. A., Hameed B. H., 2018. Photocatalytic degradation of pollutants in petroleum refinery wastewater by TiO_2- and ZnO-based photocatalysts: Recent development, *Journal of Cleaner Production*, 205, 930-954.

Bakbolat B., Daulbayev C., Sultanov F., Beissenov R., Umirzakov A., Mereke A., Bekbaev A., Chuprakov I., 2020. Recent Developments of TiO_2-Based Photocatalysis in the Hydrogen Evolution and Photodegradation: A Review, *Nanomaterials*, 10 (9), 1790.

Bindu P., Thomas S., 2014. Estimation of lattice strain in ZnO nanoparticles: X-ray peak profile analysis, *Journal of Theoretical and Applied Physics*, 8 (4), 123-134.

Bond G. C., Thompson D. T., 1999. Catalysis by Gold, *Catalysis Reviews*, 41 (3-4), 319-388.

Chen C., Yu B., Liu P., Liu J.-F., Wang L., 2011. Investigation of nano-sized ZnO particles fabricated by various synthesis routes, *Journal of Ceramic Processing Research*, 12(4), 420-425.

Clarke B., Ghandi K., The Interplay of Growth Mechanism and Properties of ZnO Nanostructures for Different Applications, *Small*, 19(44), 2302864.

Collins T. J., 2007. ImageJ for microscopy, *BioTechniques*, 43 (1S), S25-S30.

Dassanayake A. C., Wickramaratne N. P., Hossain M. A., Perera V. S., Jeskey J., Huang S. D., Shen H., Jaroniec M., 2019. Prussian blue-assisted one-pot synthesis of nitrogen-doped mesoporous graphitic carbon spheres for supercapacitors, *Journal of Materials Chemistry A*, 7 (38), 22092-22102.

Etafo N. O., Bamidele M. O., Bamisaye A., Alli Y. A., 2024. Revolutionizing photocatalysis: Unveiling efficient alternatives to titanium (IV) oxide and zinc oxide for comprehensive environmental remediation, *Journal of Water Process Engineering*, 62, 105369.

Ghosh N., Patra M., Halder G., 2024. Current advances and future outlook of heterogeneous catalytic transesterification towards biodiesel production from waste cooking oil, *Sustainable Energy Fuels*, 8 (6), 1105-1152.

Hariharan C., 2006. Photocatalytic degradation of organic contaminants in water by ZnO nanoparticles: Revisited, *Applied Catalysis A: General*, 304, 55-61.

Hossain M. A., Kayes M. N., Hossain M. M., 2021. Removal of Remazol Red RR from Aqueous Solution by Glass Supported Films of Synthesized ZnO Nanoparticles, *ICRRD Quality Index Research Journal.*, 2 (3), 109-119.

Hossain M. M., Hossain M. A., Kayes M. N., Halder D., 2014. ZnO Mediated Photodegradation of Aqueous Solutions of Crystal Violet and Ponceau S by Visible Light, *Journal of Engineering Science*, 5 (1), 69-74.

Kaschner A., Haboeck U., Strassburg M., Strassburg M., Kaczmarczyk G., Hoffmann A., Thomsen C., Zeuner A., Alves H. R., Hofmann D. M., Meyer B. K., 2002. Nitrogen-related local vibrational modes in ZnO:N, *Applied Physics Letters*, 80 (11), 1909-1911.

Kayani Z. N., Saleemi F., Batool I., 2015. Effect of calcination temperature on the properties of ZnO nanoparticles, *Applied Physics A*, 119 (2), 713-720.

Kayes M. N., Miah M. J., Obaidullah M., Hossain M. A., Hossain M. M., 2016. Immobilization of ZnO Suspension on Glass Substrate to Remove Filtration During the Removal of Remazol Red R from Aqueous Solution, *Journal of Advances in Chemistry*, 12, 4127-4133.

Khalid A., Ahmad P., Memon R., Gado L. F., Khandaker M. U., Almukhlifi H. A., Modafer Y., Bashir N., Abida O., Alshammari F. A., Timoumi A., 2023. Structural, Optical, and Renewable Energy-Assisted Photocatalytic Dye Degradation Studies of ZnO, CuZnO, and CoZnO Nanostructures for Wastewater Treatment. *Separations*, 10, 184.

Khan S. T., Al-Khedhairy A. A., Musarrat J., 2015. ZnO and TiO_2 nanoparticles as novel antimicrobial agents for oral hygiene: a review, *Journal of Nanoparticle Research*, 17 (6), 276.

Kołodziejczak-Radzimska A., Jesionowski T., 2014. Zinc Oxide-From Synthesis to Application: A Review, *Materials (Basel, Switzerland)*, 7 (4), 2833-2881.

Kumar S., Sahare P. D., 2012. Observation of band gap and surface defects of ZnO nanoparticles synthesized via hydrothermal route at different reaction temperature, *Optics Communications*, 285 (24), 5210-5216.

Lal M., Sharma P., Ram C., 2021. Calcination temperature effect on titanium oxide (TiO_2) nanoparticles synthesis, *Optik*, 241, 166934.

Lévay K., Tóth K. D., Kárpáti T., Hegedűs L., 2020. Heterogeneous Catalytic Hydrogenation of 3-Phenylpropionitrile over Palladium on Carbon, *ACS Omega*, 5 (10), 5487-5497.

Lin K.-F., Cheng H.-M., Hsu H.-C., Hsieh W.-F., 2006. Band gap engineering and spatial confinement of optical phonon in ZnO quantum dots, *Applied Physics Letters*, 88 (26), 263117.

Lin K.-F., Cheng H.-M., Hsu H.-C., Lin L.-J., Hsieh W.-F., 2005. Band gap variation of size-controlled ZnO quantum dots synthesized by sol–gel method, *Chemical Physics Letters*, 409 (4), 208-211.

Liu P. S., Chen G. F., 2014. "Chapter Two - Making Porous Metals" In book *Porous Materials*, 1st Edition, Oxford, Butterworth-Heinemann, , pp 21-112.

Mountrichas G., Pispas S., Kamitsos E. I., 2014. Effect of Temperature on the Direct Synthesis of Gold Nanoparticles Mediated by Poly(dimethylaminoethyl methacrylate) Homopolymer, *The Journal of Physical Chemistry C*, 118 (39), 22754-22759.

Ng K. H., Yuan L. S., Cheng C. K., Chen K., Fang C., 2019. TiO_2 and ZnO photocatalytic treatment of palm oil mill effluent (POME) and feasibility of renewable energy generation: A short review, *Journal of Cleaner Production*, 233, 209-225.

Ong C. B., Ng L. Y., Mohammad A. W. 2018. A review of ZnO nanoparticles as solar photocatalysts: Synthesis, mechanisms and applications, *Renewable and Sustainable Energy Reviews*, 81, 536-551.

Qin H., Li W., Xia Y., H, T., 2011. Photocatalytic Activity of Heterostructures Based on ZnO and N-Doped ZnO, *ACS Applied Materials & Interfaces*, 3 (8), 3152-3156.

Roth A. P., Webb J. B., Williams D. F., 1982. Band-gap narrowing in heavily defect-doped ZnO, *Physical Review B*, 25 (12), 7836-7839.

Tang Z., Chen Y., Ye W., 2020. Calculation of Surface Properties of Cubic and Hexagonal Crystals through Molecular Statics Simulations, *Crystals*, 10 (4), 329.

Tsai C.-Y., Lai J.-D., Feng S.-W., Huang C.-J., Chen C.-H., Yang F.-W., Wang H.-C., Tu L.-W., 2017. Growth and characterization of textured well-faceted ZnO on planar Si(100), planar Si(111), and textured Si(100) substrates for solar cell applications, *Beilstein Journal of Nanotechnology*, 8, 1939-1945.

Velusamy K., Devanand J., Kumar P. S., Soundarajan K., Sivasubramania V., Sindhu J., Vo, D.-V. N., 2021. A review on nano-catalysts and biochar-based catalysts for biofuel production, *Fuel*, 306, 121632.

Venu Gopal V. R., Kamila S., 2017. Effect of temperature on the morphology of ZnO nanoparticles: a comparative study, *Applied Nanoscience*, 7 (3), 75-82.

Wang L.-X., Guan E., Wang Z., Wang L., Gong Z., Cui Y., Yang Z., Wang C., Zhang J., Meng X., Hu P., Gong X.-Q., Gates B. C., Xiao F.-S., 2020. Dispersed Nickel Boosts Catalysis by Copper in CO_2 Hydrogenation, *ACS Catalysis*, 10 (16), 9261-9270.

Xiong G., Pal U., Serrano J. G., Ucer K. B., Williams R. T., 2006. Photoluminesence and FTIR study of ZnO nanoparticles: the impurity and defect perspective, *physica status solidi c*, 3 (10), 3577-3581.

Xu J., Teng Y., Teng F., 2016. Effect of Surface Defect States on Valence Band and Charge Separation and Transfer Efficiency, *Scientific Reports*, 6 (1), 32457.

Xu W., Kong J. S., Yeh Y.-T. E., Chen P., 2008. Single-molecule nanocatalysis reveals heterogeneous reaction pathways and catalytic dynamics, *Nature Materials*, 7, 992.

Zhou X., Xu W., Liu G., Panda D., Chen P., 2010. Size-Dependent Catalytic Activity and Dynamics of Gold Nanoparticles at the Single-Molecule Level, *Journal of the American Chemical Society*, 132 (1), 138-146.